PCCP

Accepted Manuscript

ROYAL SOCIETY OF CHEMISTRY

www.rsc.org/pccp

TOC

The photophysical properties of CIGS thin films, prepared by solution-based coating methods, are investigated to understand the correlation between the optical properties and the electrical characteristics of solar cells.

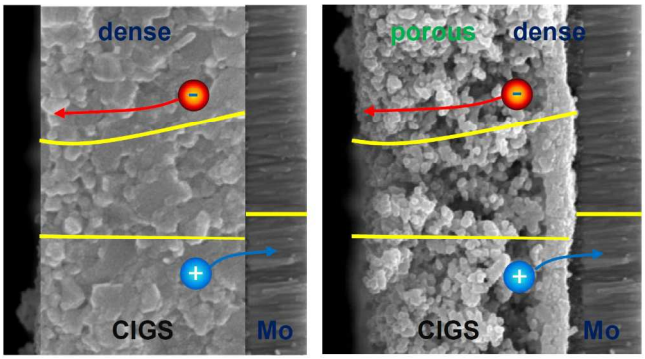

Journal Name

RSCPublishing

ARTICLE

Band gap grading and photovoltaic performance of solution-processed Cu(In,Ga)S_2 thin-film solar cells

Cite this: DOI: 10.1039/xoxxoooooox

So Hyeong Sohn,[a] Noh Soo Han,[a] Yong Jin Park,[a] Seung Min Park,[a] Hee Sang An,[b,c] Dong-Wook Kim,[d] Byoung Koun Min,*[b,c] and Jae Kyu Song*[a]

Received ooth January 2012,
Accepted ooth January 2012

DOI: 10.1039/xoxxoooooox

www.rsc.org/

The photophysical properties of $CuIn_xGa_{1-x}S_2$ (CIGS) thin films, prepared by solution-based coating methods, are investigated to understand the correlation between the optical properties of these films and the electrical characteristics of solar cells fabricated using these films. Photophysical properties, such as the depth-dependent band gap and carrier lifetime, turn out to be at play in determining the energy conversion efficiency of solar cells. A double grading of the band gap in CIGS films enhances solar cell efficiency, even when defect states disturb carrier collection by non-radiative decay. The combinational stacking of different density films leads to improved solar cell performance as well as efficient fabrication because a graded band gap and reduced shunt current increase carrier collection efficiency. The photodynamics of minority-carriers suggests that the suppression of defect states is a primary area of improvement in CIGS thin films prepared by solution-based methods.

1. Introduction

$CuIn_xGa_{1-x}S_ySe_{2-y}$ (CIGSSe) solar cells have been considered as an alternative to silicon solar cells owing to the high energy conversion efficiency and competitive fabrication cost.[1,2] Indeed, highly efficient CIGSSe solar cells (~20%) is fabricated with an absorber film thickness of only ~2 μm.[2] CIGSSe has a direct band gap and a high absorbance. Another advantage is its easily tunable band gap, which is a promising feature for tandem solar cell architecture.[3] Moreover, wide-band-gap affords high voltage to photovoltaic devices, which is advantageous for enhancing solar cell efficiency.[4,5] The band gap of CIGSSe is influenced by the composition variation and strain in its layers.[6-8] This band gap change in the absorber film can affect the collection and recombination of photocarriers, suggesting that it is feasible to improve solar cell performance by the introduction of a properly graded band gap in the absorber layer.[9,10] Solar cell efficiency is also related to the lifetime of minority-carriers,[11,12] which is determined by the various radiative and non-radiative decay channels of photo-excited carriers. In this regard, a detailed understanding of the correlation between the optical properties of absorber films and the electrical characteristics of solar cells using these films is crucial for the optimization of solar cells.

CIGSSe thin films have been fabricated by vacuum-based processes such as co-evaporation and sputtering. Recently, solution-based methods have been developed for achieving large-scale and low-cost production.[13-18] However, solution-based methods suffer from low quality of thin films and concomitant low efficiency of solar cells. In addition, solution properties significantly affect photovoltaic performance, although solution-based methods have recently become competitive even in terms of efficiency. For example, CIGSSe films prepared using hydrazine-solution-based methods resulted in high solar cell efficiency (> 15%),[13] whereas some films prepared using nanocrystalline-based methods resulted in low efficiency (< 1%).[14]

In this study, we investigate the correlation between the optical properties of $CuIn_xGa_{1-x}S_2$ (CIGS) thin films and the electrical characteristics of solar cells fabricated using these films. We used two different paste solutions to prepare CIGS thin films. One precursor paste resulted in a densely packed CIGS films, whereas the other led to a high degree of porosity in the films.[19,20] The depth-dependence of the band gap in the films indicated that a graded band gap in the dense film improved solar cell efficiency by enhanced carrier collection. Moreover, combinational stacking of layers prepared using the two pastes also affected the photovoltaic performance of solar cells, where the solar cell with dense-back and porous-front layers showed higher efficiency than that with a reversely stacked structure.[20] The band gap structure suggested the existence of a graded band gap in stacked absorber layers, which explained the enhanced solar cell efficiency. The lifetime of photo-excited carriers was shorter in the solution-processed film than that in a conventional vacuum-processed film.

2. Experimental

2.1. Preparation of pastes. *Paste A*: A precursor solution was prepared by dissolving $Cu(NO_3)_2{\cdot}xH_2O$, $In(NO_3)_3{\cdot}xH_2O$, and $Ga(NO_3)_3{\cdot}xH_2O$ in methanol, to which polyvinyl acetate was added as a binder material.[19] After stirring the precursor solution for 30 min, a paste was obtained with a viscosity of 15 ± 5 cP at 25 °C, which was suitable for spin-coating. *Paste B*: A precursor solution was prepared by dissolving $Cu(NO_3)_2{\cdot}xH_2O$, $In(NO_3)_3{\cdot}xH_2O$, and $Ga(NO_3)_3{\cdot}xH_2O$ in anhydrous ethanol. Terpineol and ethyl cellulose were added as binder materials. After condensing the solution, a paste was obtained with a viscosity of 4000 ± 100 cP at 25 °C. The viscosity difference between the two pastes was mainly attributed to the properties of the binder materials.

2.2. Fabrication of CIGS thin-film solar cells. Paste A was spin-coated and dried on a Mo-coated glass substrate; this process was repeated about six times to obtain the desired thickness for the dense film (~1.2 μm).[19] After coating and drying, air annealing was performed under ambient conditions to remove the binder materials, which resulted in a mixed oxide film of Cu, In, and Ga. Then, sulfurization of the oxide film was carried out in a H_2S/N_2 gas environment, which resulted in the formation of the dense CIGS film. The porous film was prepared via a single cycle of spin-coating and drying owing to the relatively high viscosity of paste B. The porous film was then subjected to two-step (oxidation and sulfurization) annealing under conditions identical to those employed for the dense film annealing. For obtaining combinational stacking with the configuration of A+B, paste A was spin-coated onto a Mo-coated glass substrate and dried under ambient conditions.[20] On top of the dried film, paste B was spin-coated and dried. The films were annealed under ambient conditions and then sulfurized in a H_2S/N_2 gas environment. For the configuration of B+A, paste B was spin-coated onto a Mo-coated glass substrate. On top of the dried film, paste A was spin-coated and dried. The dried film was then subjected to two-step (oxidation and sulfurization) annealing under conditions identical to those employed in the case of A+B. Solar cell devices were fabricated with a conventional configuration (Mo/CIGS/CdS/*i*-ZnO/*n*-ZnO/Ni/Al).

2.3. Characterization of CIGS films. Structural characterization of the films was performed using a scanning electron microscope (SEM).[19] Composition analysis was carried out using an electron probe microanalyzer (EPMA), energy-dispersive X-ray spectroscopy (EDX), and Auger electron spectroscopy (AES). Absorbance of the films was measured using a diffuse reflectance UV-vis spectrophotometer (Cary 5000, Varian). For obtaining steady-state and time-resolved photoluminescence spectra, CIGS films were excited by the fundamental wavelength of a cavity-dumped oscillator (Mira/PulseSwitch, Coherent, 1 MHz, 710 nm, 150 fs). The CIGS films were held in a cryostat (CCR, Janis) in which the temperature was varied from 10 to 300 K by using a temperature controller (331, LakeShore). Emission from the films was collected using a set of lens, spectrally resolved using a monochromator, detected using a photomultiplier, and recorded using a time-correlated single photon counter (TCSPC, PicoHarp, PicoQuant). The instrumental response of the entire system was 0.05 ns.[21,22] Solar cell performances were characterized using a class-AAA solar simulator (Wacom) and an incident photon conversion efficiency (IPCE) measurement unit (McScience).

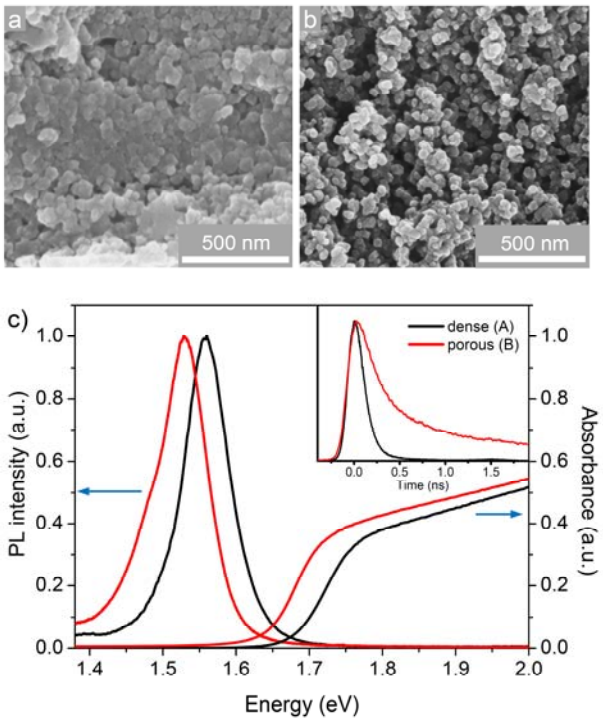

Fig. 1 (a) Scanning electron microscopy (SEM) image of CIGS film prepared using paste A shows a densely packed morphology (cross-sectional view). (b) SEM image of CIGS film prepared using paste B shows a porous morphology (cross-sectional view). (c) Absorption and photoluminescence spectra indicate that the band gap energy of the dense film (paste A) is slightly higher than that of the porous film (paste B). The inset shows the time profiles of time-resolved photoluminescence at 820 nm. Intensities are normalized for comparison purposes.

3. Results and discussion

3.1. Band gap structures in CIGS films

The two paste solutions (paste A and B with a viscosity of 15 ± 5 cP and 4000 ± 100 cP at 25 °C, respectively) were used to prepare CIGS thin films. The films prepared using paste A showed a densely packed morphology (Fig. 1a) and a high energy conversion efficiency (ECE) of 8.3%.[19] On the other hand, the films prepared using paste B revealed a high degree of porosity (Fig. 1b) and a relatively low ECE of < 3%. To understand these differences, the photophysical properties of the different density films were investigated. The band gap energy (E_g) of the films could be estimated from their absorption spectra, which indicated E_g of ~1.7 eV (Fig. 1c). However, E_g could not be easily assigned from the absorption spectra, because the exciton absorption was not clearly discernible. In addition, E_g was in the non-negligible range of uncertainty (~0.05 eV), when E_g was estimated by extrapolating the linear portion of the absorption slope in the spectra, due to the

smooth onset of absorbance and the absence of the exciton absorption band. Alternatively, E_g was examined from the photoluminescence spectrum of the films, because the photoluminescence of direct-band-gap materials indicated the near-band-edge transition and thus implied E_g of these materials. However, the value of E_g estimated from the photoluminescence spectrum was different from the absorption spectrum (~0.15 eV), which was attributed to the Stokes shift, because this range of the Stokes shift was frequently observed in CIGS.[23,24]

E_g of the dense film (paste A) was slightly higher than that of the porous film (paste B) in both absorption and photoluminescence spectra (Fig. 1c). At first, the composition variation of the CIGS films was assumed to result in the difference in E_g (~0.03 eV). The AES analysis indicated that the chemical composition ([Cu]/[In]/[Ga]) was 1:~0.7:~0.3 in the dense films, which agreed with the spin-casted composition ratio of 1:0.7:0.3 onto the Mo-coated glass substrate.[19] In this composition ratio, E_g was expected to be ~1.7 eV by the linear approximation model,[25,26] which agreed with E_g estimated from the absorption spectrum. In addition, EDX analysis showed that the composition ([Cu]/[In]/[Ga]/[S]) was 1:0.75:0.29:2.07 in the dense films. It is notable that In rich and Ga poor composition was also observed in some selected region of the films, which was supported by EPMA analysis.[19] These results implied that the composition was not homogeneous in the dense films, which will be discussed in the following. Nevertheless, the overall composition ratio in the dense films was similar to that in the porous films within the error range of AES, EDX, and EMPA, since the precursor mixture solutions of both paste A and B included identical amounts of $Cu(NO_3)_2{\cdot}xH_2O$, $In(NO_3)_3{\cdot}xH_2O$, and $Ga(NO_3)_3{\cdot}xH_2O$. In this regard, the composition variation could not explain the difference in E_g between the dense and porous films.

Instead, the difference in E_g was attributed to the morphology difference of grains. The average grain size in the dense film was smaller than that in the porous film,[19] although the coalescence of small grains typically occurred in the dense film. In other words, the quantum confinement effect might be at play, although the confinement effect was not significant in this size regime,[27,28] because the grain size was larger than the exciton Bohr radius. Indeed, the small variation of E_g (0.03 eV) was observed in SnO_2 nanocrystalline films, even when the grain size was larger than the exciton Bohr radius,[29,30] which happened to match the observed ΔE_g between the dense and porous films. In addition, the effect of the grain size was observed in the lifetimes of photo-excited carriers. In the dense film, the lifetime was about 0.2 ns (inset of Fig 1c), while that in the porous film was 0.9 ns. In the dense film, the large surface area of the small grains resulted in surface-related defect states and concomitant non-radiative decay to the defect states, which reduced the lifetimes of photocarriers and thus the emission intensities.

The morphology difference also led to the different penetration depth of incident light. Since the absorbance of CIGS was large ($\alpha \approx 10^5$ cm^{-1}) for photon energies above the band gap,[31,32] most (90%) of incident light (710 nm) was absorbed within the depth of 230 nm. On the other hand, the relatively large pores allowed a deeper penetration depth in the porous film than the dense film. Since the low-lying layer had a smaller value of E_g than the surface layer, which will be discussed in the following, the deeper penetration depth resulted in a smaller value of E_g in the porous films. Accordingly, both grain sizes and penetration depths were responsible for the difference in E_g between the dense and porous films, although the contribution of each factor could not be separated.

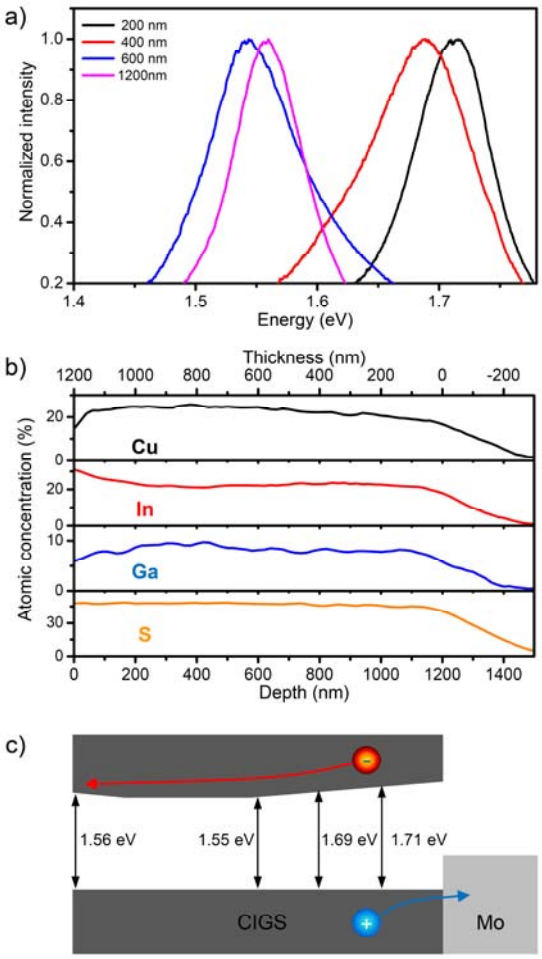

Fig. 2 (a) Photoluminescence spectra of the dense film indicate that the band gap energy changes as a function of thickness. Intensities are normalized for comparison purposes. (b) Composition profiles in the dense film are obtained by Auger depth profiling. (c) The depth-dependent band gap energy is schematically represented by the shift in the conduction band minimum, which shows a double grading of the band gap structure.

Since the band gap structure was known to influence the solar cell efficiency,[9,10] E_g was investigated as a function of film thickness using the photoluminescence spectra. The information depth of the photoluminescence spectrum, which is defined as the depth that 90% of the overall signals were obtained, was ~230 nm.[31,32] Therefore, E_g near the surface layer (depth range of 50 nm) was corrected from the measured photoluminescence *via* weighting by the exponential attenuation function, because the photoluminescence intensity was governed by an exponential attenuation. Accordingly,

photoluminescence indicated the depth-dependent band gap structure more clearly than absorbance did.

In the dense films, the variation of E_g was not monotonous as a function of thickness (Fig. 2a). E_g of the thinnest film (200 nm) was the highest (1.71 eV), and it decreased to 1.69 eV at a thickness of 400 nm. The change in E_g could not be explained by the composition variation of the CIGS films, because the compositions of elements, obtained from Auger depth profiling, were similar in this regime (Fig. 2b).[19] Instead, the higher E_g value for the thinnest film was attributed to the chemical interaction and strain distribution effect at the CIGS/Mo interface.[6-8] It was observed that the back (bottom) sides of CIGSSe thin films showed higher E_g than their front (top) sides due to the chemical interaction with the Mo interface, where the difference was as large as 0.20 eV.[6] Furthermore, the difference in E_g was also related to substrate-induced strain, which increased E_g by 0.05 eV.[8] Accordingly, E_g decreased to 1.55 eV with an increase in thickness (~600 nm), because the effect of the chemical interaction and strain became weaker. Indeed, the difference in E_g was 0.16 eV between the back and central regions, which could be explained by the chemical interaction and strain effect at the interface.

With further increase in thickness (> 600 nm), E_g did not change significantly, while a slight increase in E_g (1.56 eV) was observed at a thickness of 1200 nm. This was ascribed to the variation of the Cu and Ga contents, when the effect in CIGS was assumed to be similar to that in CIGSSe, because this effect in CIGS has not been reported. The Ga content decreased with an increase in thickness (> 1000 nm), which expected the decrease in E_g by 0.05 eV.[33] The Cu content also decreased in this regime, which expected the increase in E_g by 0.04 eV.[32] In this regard, it is suggested that the reduced Ga content was counter-balanced by the deficiency in the Cu content, which resulted in slight increase in E_g at a thickness of 1200 nm. It is noted that the slight decrease in E_g was expected in above estimation, because the decrease of 0.05 eV (Ga content) was compensated by the increase of 0.04 eV (Cu content). This discrepancy might be related to the approximation using the composition variation in CIGSSe, which might not be identical to that in CIGS. In this regard, the photoluminescence spectra and Auger depth profiling indicated that E_g changed as a function of thickness in the CIGS films.

Generally, the valence band maximum was slightly affected by the change of E_g.[9,10] Indeed, the valence band maximum was observed to be nearly flat between the back and front sides, when E_g was significantly affected by the chemical interaction at interface.[6] Accordingly, the change of E_g in CIGS films could be represented by a shift of the conduction band minimum. Interestingly, the depth-dependence of E_g indicated a double grading of the conduction band minimum in the dense films, as schematically shown in Fig. 2c. The simulation study indicated that the double grading enhanced the ECE by ~30%, compared to the flat one, due to the influence on the dynamics of the minority charge carriers (electron).[9] High E_g at the back side afforded the graded band gap, which increased the minority-carrier diffusion length and improved the short circuit current (J_{sc}). High E_g at the front side usually reduced the recombination rate in the space charge region, because the barrier height became higher by the widened band gap, where a high open circuit voltage (V_{oc}) was also expected. On the other hand, the anti-grading at the front layer (~0.01 eV) could act as a barrier for minority-carrier collection. However, the barrier effect was not apparent, because the thermal energy (> 0.02 eV) was sufficient for minority-carriers to overcome the barrier. Therefore, the double grading led to the high values of V_{oc} and J_{sc} in the dense films, which afforded the high ECE of solar cells (Table 1).

Table 1. Measured band gap energies of absorber films and performance values of CIGS thin-film solar cell devices

sample	E_g (eV)	V_{oc} (mV)	J_{sc} (mA/cm^2)	FF (%)	η (%)
A	1.56	787	17.0	61.9	8.28
B	1.53	477	11.5	52.7	2.90
A+B	1.53	537	14.4	60.2	4.66
B+A	1.56	572	8.1	58.1	2.71

It should be noted that the lifetime of the minority-carriers was 0.2 ns in the dense films, which was shorter than the reported ones (~10 ns) in high-performance CIGS solar cells.[11,12] The small grains in the dense film were prepared by solution-based methods, although the coalescence of grains was observed. Thus the short lifetimes were attributed to non-radiative decay to surface-related defect states, which implied that the improvement of minority-carrier lifetimes would increase the solar cell efficiency further. In this regard, efficient carrier collection was explained by the graded band gap for minority-carriers, which improved the minority-carrier diffusion length, although non-radiative decay might have reduced the diffusion length.

The depth-dependence of E_g was also investigated in the porous films (Fig. 3a). In fact, E_g at the back layer near Mo substrates could not be estimated, because the thin film (< 500 nm) was not prepared due to the high viscosity of paste B. In the possibly prepared thinnest film (~500 nm), E_g was 1.51 eV, which slightly increased to 1.53 eV with an increase in the film thickness (1200 nm). The change of E_g was attributed to the composition variation (Fig. 3b). The Cu content decreased with an increase in thickness (> 500 nm), which led to a higher E_g at the front side.[32] On the other hand, the Ga content was not changed much in this regime, which was different from the dense films. Indeed, the anti-grading at the front side was slightly larger in the porous films (0.02 eV) than the dense films (0.01 eV), which was correlated to the variation of the Ga content in the porous films. Although E_g at the back side was not directly measured, E_g at the back side would be larger than that at the front side, because the chemical interaction and strain would affect E_g at the CIGS/Mo interface of the porous films.[6-8] Indeed, the back side of the dense films was observed to have higher E_g than the front side due to the chemical interaction with the Mo interface as well as the substrate-induced strain. Accordingly, it was assumed that E_g would increase with a decrease in thickness of the porous films, because the effect of the chemical interaction and strain became stronger.

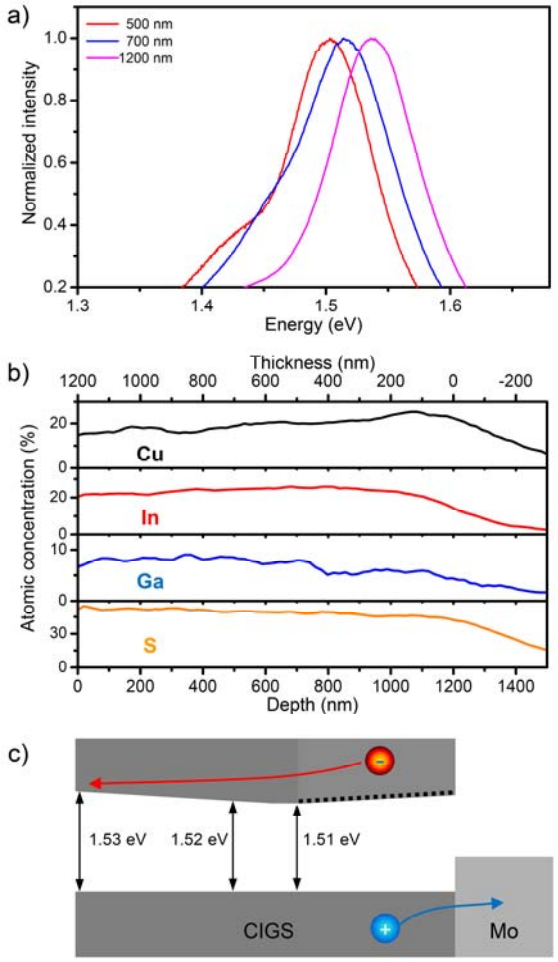

Fig. 3 (a) Photoluminescence spectra of the porous film indicate that the band gap energy slightly increases with an increase in thickness (> 500 nm). (b) The composition profiles are obtained in the porous film by Auger depth profiling. (c) The depth-dependent band gap energy is schematically. Dotted line is assumed to take the chemical interaction and strain at the CIGS/Mo interface into account.

The band gap structure in the porous films (Fig. 3c) was not much different from that in the dense films, although E_g at the back side was assumed at this point. Thus a low ECE could not be explained by the depth-dependence of E_g in the porous films. In addition, the relationship between E_g and V_{oc} in the porous films was not similar to that in the dense films. In other words, E_g at the front layer of the porous films was slightly smaller (0.03 eV) than that of the dense films, although V_{oc} of the porous films was significantly smaller (0.31 V) than that of the dense films (Table 1). Generally, V_{oc} was affected by shunt leakage current, which was related to the diffusion of contact metal through the buffer and window layers at localized regions in CIGS solar cells.[34,35] Since the buffer (CdS) and window (ZnO) layers were very thin in this study, the porosity of CIGS films could lead to pinhole-like faults, where the localized diffusion of the contact metal could induce shunt current. Indeed, the shunt resistance in the porous films was less than half of that in the dense films,[19] which indicated that the porosity of films was responsible for the shunt current. Therefore, it was concluded that the effect of porosity was predominant over the band gap structures in the solar cell prepared using paste B.

3.2. Band gap structures in combinational stacking of layers

The dense films with higher solar cell efficiency required multiple coating-and-drying cycles to achieve a proper film thickness, which might restrict the low-cost production of the solar cells. On the other hand, the porous films with a similar thickness, which were prepared by a single coating process, resulted in lower efficiency. In this regard, a combination of paste A and B was expected to provide efficient fabrication and improve the solar cell performance. For a combination of pastes with the configuration of A+B, a thin dense layer (200 nm) was prepared using a single coating of paste A, which was followed by a single coating of paste B for a thick porous layer (1000 nm).[20] Certainly, a dense layer was observed at the bottom of the film (Fig. 4a), which indicated that the layer density was not affected by sequential stacking. Likewise, the configuration of B+A indicated that the porous layer was deposited prior to the dense layer (Fig. 4b).

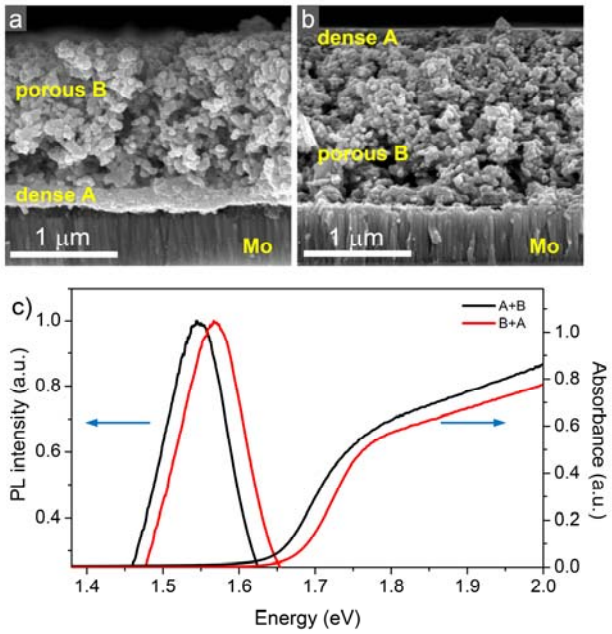

Fig. 4 (a) SEM image shows the CIGS thin film of the configuration of A+B (cross-sectional view), where the dense layer is in the bottom and the porous layer lies above it. (b) SEM image shows the CIGS thin film of the configuration of B+A (cross-sectional view), where the porous layer is in the bottom of the film and the dense layer lies above it. (c) Absorption and photoluminescence spectra indicate that the band gap energy of A+B is slightly lower than that of B+A.

Photoluminescence and absorption spectra indicated that the measured E_g value for A+B was smaller than that for B+A (Fig. 4c). Since the observed photoluminescence was mainly governed by the front layer, the measured E_g of A+B (1.53 eV) primarily reflected E_g of the front porous layer. It is notable that sequential stacking did not change E_g of the front porous layer considerably, which agreed with the observation that the crystal structure and layer density were not

influenced by stacking.[20] Similarly, V_{oc} of the solar cell of A+B (537 mV) was lower than that of B+A (572 mV), because V_{oc} was mainly affected by E_g of the front layer. Indeed, the difference in V_{oc} between A+B and B+A (35 mV) was similar to the difference in E_g between A and B (30 meV), although other factors such as shunt current and carrier recombination also influenced V_{oc}, as discussed above.

The double grading of the band gap structure was expected in A+B (Fig. 5a), when the depth-dependence of E_g was assumed to be unaffected by stacking, as in the case of the front layer. The higher E_g value at the back layer afforded the graded band gap and increased J_{sc} (Table 1). Notably, V_{oc} and J_{sc} of A+B were significantly improved from the porous film prepared using paste B, even though most (~80%) of films in A+B were porous layer. The dense layer in A+B would reduce the shunt current considerably, which increased the ECE of A+B up to 4.7%. Moreover, two cycles of coating-and-drying process in A+B, which was simplified from six cycles in the dense films prepared using paste A, would facilitate the low-cost production of the solar cells.

The ECE of B+A, however, was not improved from the porous film, which was attributed to the low value of J_{sc}. At first, the anti-grading of the band gap structure at the front layer (Fig. 5b) was responsible for the low J_{sc} value. Indeed, the external quantum efficiency of B+A was significantly enhanced at long wavelengths (> 700 nm) in the reverse bias condition,[20] supporting the presence of the anti-graded band gap. Moreover, the anti-grading barrier (~0.05 eV) was larger than the thermal energy, which disturbed the minority-carrier collection. Second, the minority-carriers in B+A was affected by the short lifetime at 300 K (Fig. 5d), which was shorter than A+B (Fig. 5c). It is notable that the lifetime of the minority-carriers in B+A was similar to that in A+B at a low temperature (10 K), but the former became significantly shorter with an increase in temperature. The temperature-dependence suggested a non-negligible amount of defect states, because non-radiative decay to defect states was suppressed at the low temperature.[36,37] In other words, the small grains in the front dense layer were responsible for the surface-related defect states and the short lifetime of minority-carriers. Accordingly, the diffusion of minority-carriers was disturbed by the short lifetime in the front layer, in addition to the anti-graded band gap, which resulted in no improvement in solar cell efficiency of B+A, compared to the porous film.

4. Conclusions

The band gap structures and the lifetimes of minority-carriers were investigated in CIGS films to understand the relationship between the photophysical properties of absorber films and solar cell efficiencies. The double-grading of the band gap in the dense films enhanced the solar cell efficiency, because high E_g at the front and back sides increased the open circuit voltage and minority-carrier diffusion length, respectively. In the porous films, the effect of the shunt current was predominant over the graded band gap, which explained the low solar cell efficiency. In the combinational stacking of A+B, the reduced shunt current as well as the graded band gap improved the solar cell efficiency. In B+A, however, the diffusion of minority-carriers was disturbed by the anti-graded band gap and the short lifetime, which resulted in no improvement in solar cell efficiency. The CIGS thin films fabricated by solution-based methods turned out to afford the band gap grading, which was vital for efficiency improvement. Finally, the improvement of minority-carrier lifetimes is needed in thin films prepared by solution-based methods for the large-scale and low-cost production application.

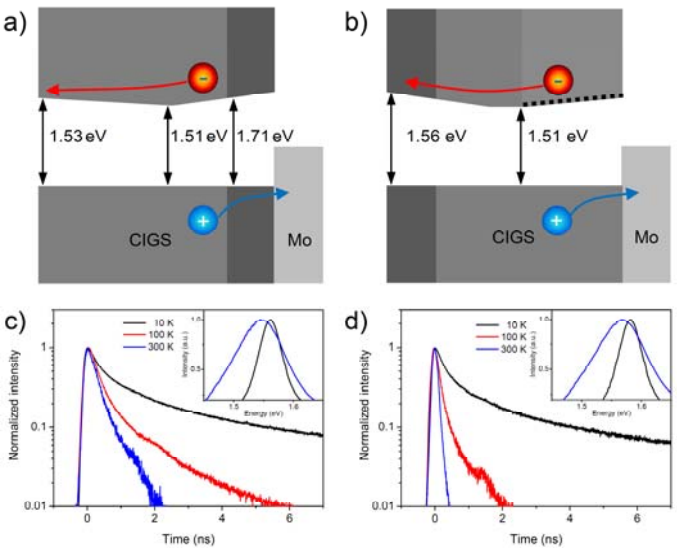

Fig. 5 (a) The depth-dependent band gap energy in the configuration of A+B is schematically represented. (b) The depth-dependent band gap energy in the configuration of B+A is represented. Dotted line is assumed to take the chemical interaction and strain at the CIGS/Mo interface into account. The decay profiles of time-resolved photoluminescence at 820 nm in (c) A+B and (d) B+A are presented as a function of temperature. The inset shows the temperature-dependent photoluminescence spectra. Intensities are normalized for comparison purposes.

Acknowledgements

This work was supported by the Basic Science Research Programs through the National Research Foundation of Korea (NRF) funded by the Ministry of Education, Science and Technology (NRF-2012R1A1A2039882) and the National Research Foundation of Korea Grant funded by the Korean Government (MEST, NRF-2009-C1AAA001-0092939).

Notes and references

[a] *Department of Chemistry, Kyung Hee University, Seoul 130-701, Korea. E-mail: jaeksong@khu.ac.kr*

[b] *Clean Energy Research Center, Korea Institute of Science and Technology, Seoul 136-791, Korea. E-mail: bkmin@kist.re.kr*

[c] *Green School, Korea University, Seoul 136-713, Korea*

[d] *Department of Physics, Ewha Womans University, Seoul 120-750, Korea*

1. S. Hegedus, *Prog. Photovoltaics*, 2006, **14**, 393-411.
2. P. Jackson, D. Hariskos, E. Lotter, S. Paetel, R. Wuerz, R. Menner, W. Wischmann and M. Powalla, *Prog. Photovoltaics*, 2011, **19**, 894-897.

3. D. L. Young, J. Abushama, R. Noufi, Xiaonan Li, J. Keane, T. A. Gessert, J. S. Ward, M. Contreras, M. Symko-Davies and T. J. Coutts, *Conference Record of the Twenty-Ninth IEEE,* 2002, 608-611.
4. A. Shah, P. Torres, R. Tscharner, N. Wyrsch and H. Keppner, *Science,* 1999, **285**, 692-698.
5. S. Siebentritt, *Thin Solid Films,* 2002, **403–404**, 1-8.
6. M. Bär, S. Nishiwaki, L. Weinhardt, S. Pookpanratana, W. N. Shafarman and C. Heske, *Appl. Phys. Lett.,* 2008, **93**, 042110.
7. M. Bär, L. Weinhardt, C. Heske, S. Nishiwaki and W. N. Shafarman, *Phys. Rev. B,* 2008, **78**, 075404.
8. A. Slobodskyy, T. Slobodskyy, T. Ulyanenkova, S. Doyle, M. Powalla, T. Baumbach and U. Lemmer, *Appl. Phys. Lett.,* 2010, **97**, 251911.
9. J. Song, S. S. Li, C. H. Huang, O. D. Crisalle and T. J. Anderson, *Solid-State Electronics,* 2004, **48**, 73-79.
10. V. Gremenok, V. Zalesski, A. Khodin, O. Ermakov, R. Chyhir, V. Emelyanov and V. Syakersky, *Phys. Status Solidi C,* 2009, **6**, 1237-1240.
11. S. Shirakata, K. Ohkubo, Y. Ishii and T. Nakada, *Solar Energy Mater. Solar Cells,* 2009, **93**, 988-992.
12. T. Nakada and S. Shirakata, *Solar Energy Mater. Solar Cells,* 2011, **95**, 1463-1470.
13. T. K. Todorov, O. Gunawan, T. Gokmen and D. B. Mitzi, *Prog. Photovoltaics,* 2013, **21**, 82-87.
14. M. G. Panthani, V. Akhavan, B. Goodfellow, J. P. Schmidtke, L. Dunn, A. Dodabalapur, P. F. Barbara and B. A. Korgel, *J. Am. Chem. Soc.,* 2008, **130**, 16770-16777.
15. C. J. Hibberd, E. Chassaing, W. Liu, D. B. Mitzi, D. Lincot and A. N. Tiwari, *Prog. Photovoltaics,* 2010, **18**, 434-452.
16. S. E. Habas, H. A. S. Platt, van Hest, Maikel F. A. M. and D. S. Ginley, *Chem. Rev.,* 2010, **110**, 6571-6594.
17. V. A. Akhavan, B. W. Goodfellow, M. G. Panthani, D. K. Reid, D. J. Hellebusch, T. Adachi and B. A. Korgel, *Energy Environ. Sci.,* 2010, **3**, 1600-1606.
18. S. Ahn, K. Kim, A. Cho, J. Gwak, J. H. Yun, K. Shin, S. Ahn and K. Yoon, *ACS Appl. Mater. Interfaces,* 2012, **4**, 1530-1536.
19. S. J. Park, J. W. Cho, J. K. Lee, K. Shin, J. Kim and B. K. Min, *Prog. Photovoltaics,* 2014, **22**, 122-128.
20. H. S. An, Y. Cho, S. J. Park, H. S. Jeon, Y. J. Hwang, D. Kim and B. K. Min, *ACS Appl. Mater. Interfaces,* 2014, **6**, 888-893.
21. N. S. Han, H. S. Shim, J. H. Seo, S. Y. Kim, S. M. Park and J. K. Song, *J. Appl. Phys.,* 2010, **107**, 084306.
22. N. S. Han, H. S. Shim, J. H. Seo, S. M. Park, B. K. Min, J. Kim and J. K. Song, *Chem. Phys. Lett.,* 2011, **505**, 51-56.
23. W.-S. Song, J.-H. Kim, J.-H. Lee, H.-S. Lee, Y. R. Do and H. Yang, *J. Mater. Chem.,* 2012, **22**, 21901-21908.
24. O. Yarema, D. Bozyigit, I. Rousseau, L. Nowack, M. Yarema, W. Heiss and V. Wood, *Chem. Mater.,* 2013, **25**, 3753−3757.
25. S.-H. Wei and A. Zinger, *J. Appl. Phys.,* 1995, **78**, 3846.
26. M. Bär, W. Bohne, J. Rőhrich, E. Strub, S. Linder, M. C. Lux-Steiner, Ch.-H. Fisher, T. P. Niesen and F. Karg, *J. Appl. Phys.,* 2004, **96**, 3857-3860.
27. L. E. Brus, *J. Chem. Phys.,* 1984, **80**, 4403-4409.
28. I. J. Kramer, L. Levina, R. Debnath, D. Zhitomirsky and E. H. Sargent, *Nano Lett*., 2011, **11**, 3701-3706.
29. E. J. H. Lee, C. Ribeiro, T. R. Giraldi, E. Longo, E. R. Leite and J. A. Varela, *Appl. Phys. Lett*., 2004, **84**, 1745-1747.
30. S. S. Pan, S. F. Yu, Y. X. Zhang, Y. Y. Luo, S. Wang, J. M. Xu, and G. H. Li, *J. Appl. Phys.,* 2013, **113**, 143104.
31. M. Bär, S. Nishiwaki, L. Weinhardt, S. Pookpanratana, O. Fuchs, M. Blum, W. Yang, J. D. Denlinger, W. N. Shafarman and C. Heske, *Appl. Phys. Lett.,* 2008, **93**, 244103.
32. S. Han, A. M. Hermann, F. S. Hasoon, H. A. Al-Thani and D. H. Levi, *Appl. Phys. Lett.,* 2004, **85**, 576-578.
33. M. I. Alonso, M. Garriga, C. A. D. Rincón, E. Hernández and M. León, *Appl. Phys. A,* 2002, **74**, 659-664.
34. S. Dongaonkar, J. D. Servaites, G. M. Ford, S. Loser, J. Moore, R. M. Gelfand, H. Mohseni, H. W. Hillhouse, R. Agrawal, M. A. Ratner, T. J. Marks, M. S. Lundstrom and M. A. Alam, *J. Appl. Phys.,* 2010, **108**, 124509.
35. I. C. Robin, B. Gauron, P. Ferret, C. Tavares, G. Feuillet, L. S. Dang, B. Gayral and J. M. Gérard, *Appl. Phys. Lett.,* 2007, **91**, 143120.
36. S. Luo and P. K. Chu, *Appl. Phys. Lett*., 2006, **88**, 183112.
37. S. S. Pan, Y. H. Tian, Y. Y. Luo, Y. X. Zhang, S. Wang and G. H. Li, *Appl. Phys. Lett*., 2010, **97**, 221105.